# An Online Event-Based Grid Impedance Estimation Technique Using Grid-Connected Inverters

Nabil Mohammed, *Student Member, IEEE*, Tamas Kerekes, *Senior Member, IEEE*, and Mihai Ciobotaru, *Senior Member, IEEE*

***Abstract*—An increasing intake of grid-connected inverters could change the characteristics of low voltage networks including the equivalent grid impedance seen by each inverter at its point of common coupling. This can impact the overall performance of the inverters, and thus it becomes necessary for grid-connected inverters to estimate the grid impedance online. However, there are some challenges when it comes to grid impedance estimation using grid-connected inverters. These include the estimation accuracy and the associated power quality issues that are mainly related to the amplitude, frequency, and time period of the injected disturbance into the grid. To address these challenges, a novel online event-based grid impedance estimation technique for grid-connected inverters is proposed in this article. This technique combines an active grid impedance estimation technique, based on variations of the inverter's output power [active (P) and reactive (Q) power variations], and the continuous monitoring of the positive-sequence amplitude of the PCC voltage. The main advantage is that the estimation technique only performs a deliberate perturbation of P and Q if there is a certain change in voltage magnitude related to grid impedance change. This will significantly reduce the occurrence of required PQ variations, thus minimizing the power losses and the impact on power quality. Simulation and experimental results of a grid-connected inverter system validate the performance of the proposed technique.**

***Index Terms*—Impedance measurement, inverters, power system identification, PQ variations, modeling, voltage monitoring.**

## I. Introduction

THE extensive integration of distributed generation units transforms the existing low-voltage (LV) distribution network from a passive to an active mode. The active mode comprises of both local power generators and loads. While this new shift enables more integration of distributed energy resources (DERs), several challenges are posed such as reverse power flow and voltage rise/drop along the feeders, especially in distribution networks with high intake of solar photovoltaic (PV) inverters. In this context, grid-connected inverters, which play a major role in the operation of such networks, can help the grid by providing ancillary services such as voltage regulation, frequency support, and LV ride-through capability. To enable such functions, it is necessary for the grid-connected inverters to estimate the grid parameters online such as grid voltage, grid frequency, and grid impedance [1], [2].

The information of grid impedance at the fundamental frequency is beneficial for the reliable operation of grid-connected inverters. It can be utilized as an additional degree of freedom for enhancing the overall performance of inverters [3]–[7]. For example, the estimated grid impedance at fundamental frequency was used for islanding detection [3], voltage control [4], reactive power support [5], decoupling the inner current loops in synchronous (*dq*) reference frame [6], and robust control of grid-connected inverters such as the adaptive tuning of the synchronous reference frame phase-locked loop (SRF-PLL) to cope with grid impedance variations [7]. Furthermore, the estimated wideband grid impedance was used for stability analysis based on generalized Nyquist criteria [8], [9], fault detection [10], and short circuit current calculation [11]. On the other hand, there are some potential challenges associated with the lack of grid impedance information. These include the risk of negative impedance instability [13] and the poor performance of the distributed generation units due to the variations of the grid impedance, especially the increase in the grid inductance [7]. While the output impedance of inverters is derived from its design specification [14], the major challenge with the grid impedance is that it is a time-varying variable and it cannot be measured directly at the point of common coupling (PCC). Hence, online estimation techniques should be adopted.

Online grid impedance estimation techniques are broadly divided into passive and active techniques. Passive techniques deploy normal system operation to estimate the grid impedance. The main advantage of these techniques is that they do not disturb the system [15]. Examples of these techniques are extended Kalman filter (EKF) [16] and recursive least squares (RLS) [3], [17], [18]. Overall, the common drawback of the passive techniques is their low estimation accuracy. Furthermore, the main challenges with EKF are the tuning process of the unknown parameters of the measurement noise covariance matrix and the process noise covariance matrix, that influence the estimation performance of the EKF algorithm. Furthermore, the implementation of RLS requires further complexity for grid synchronization [17] and communication [18].

In contrast, active grid impedance estimation techniques intentionally disturb the grid and then perform data acquisition

Manuscript received February 26, 2020; revised July 20, 2020; accepted September 29, 2020. Date of publication October 9, 2020; date of current version January 22, 2021. Recommended for publication by Associate Editor R. Burgos. *(Corresponding author: Nabil Mohammed.)*

Nabil Mohammed and Mihai Ciobotaru are with the School of Engineering, Macquarie University, Sydney, NSW 2109, Australia (e-mail: nabil.mohammed@ieee.org; ciomih@ieee.org).

Tamas Kerekes is with the Department of Energy Technology, Aalborg University, 9220 Aalborg, Denmark (e-mail: tak@et.aau.dk).

Color versions of one or more of the figures in this article are available online at https://ieeexplore.ieee.org.

Digital Object Identifier 10.1109/TPEL.2020.3029872

and signal processing. They provide more accurate results compared to the passive techniques [15]. Active techniques include, for example, frequency-based injection techniques, where the injected disturbance signal could be: 1) a single frequency at 600 [19], 300 [5], or 75 Hz [4]; 2) dual frequencies at 400 and 600 Hz [19]; or 3) a large spectrum of frequencies which include pseudorandom binary sequence (PRBS) [8], [9], [21]. Active techniques also include current impulse injection [7] and transient voltage injection [20]. The common drawbacks of the active techniques are: 1) additional injected disturbance to the grid which may lead to power quality issues; 2) complex postprocessing of the acquired data which usually involves discrete Fourier transform (DFT); 3) long estimation time required to obtain accurate estimation results, for instance, the need to generate the PRBS with low-frequency resolution; and 4) high magnitude of the injected impulse disturbances, which could affect the estimation accuracy due to excitation of the system nonlinearity.

Apart from the abovementioned active techniques, grid impedance estimation based on variations of the inverter's output power (PQ variations) has gained more interest due to its simple implementation and highly reduced computational burden [22]–[27]. This technique was proposed initially by [22] for a single-phase grid connected system controlled in the stationary reference frame ($\alpha\beta$-axis). This technique relied on two operating points sampled at specific instances during the active and reactive power (PQ) variations. A similar approach was presented in [23] and [24] for three-phase grid-connected inverter systems. For inverters controlled in the synchronous reference frame (*dq* reference frame), authors of [25] and [26] proposed new methodologies based on four operating points for PQ variations to minimize the effects of the inherent *dq* reference frame coupling, thus improving the estimation accuracy. However, the major drawbacks with these techniques include: 1) decreasing the energy yield of the distributed generation units due to the need to set the active power to zero while estimating the grid inductance, and setting the reactive power to zero while estimating the grid resistance; and 2) increasing the estimation time when compared to two operating points method.

Recently, a new PQ variations technique based on three operating points was proposed as a tradeoff between the estimation accuracy and the required estimation time for inverters controlled in the *dq* reference frame [27]. The main advantage is that it does not require to set the active or reactive power to zero during the estimation. This technique was embedded into *dq* reference frame of a positive- and negative-sequence control (PNSC) strategy to cope with the unbalanced operation. However, the performance of this technique was tested using simulation only. Additionally, all the above studies on grid impedance estimation using PQ variations have a common drawback of applying periodic PQ variations, which is 1) unnecessary if there are no changes in the impedance; and 2) it may lead to voltage flickers in presence of multiple inverters using the same technique.

Even though the typical equivalent grid impedance at any given point along a feeder is a time-varying parameter with clear day- and night-time patterns [28] and [29], its value varies occasionally rather than continuously over the time. In normal operation, the causes of such variations are predominantly related to changes in the output power of DERs and load profile. Therefore, as a tradeoff between the active and the passive grid impedance estimation techniques using grid-connected inverters, recent works propose hybrid/event-based grid impedance estimation strategies. The authors of [30], proposed a hybrid estimation technique based on a Luenberger observer to trigger the pulsed signal injection when a grid impedance change is detected. Even though this led to a significant reduction in the distortion time, a more complex grid impedance estimation was used since it deployed an observer, pulsed signal injection, and RLS. A parametric estimation technique for grid admittance based on pulsed signal injection was also proposed in [31]. This is a hybrid technique that relies on sensitivity analysis to inject the required disturbance signal to the grid.

Nevertheless, the hybrid grid impedance estimation techniques in both [30] and [31] still required frequency-based disturbance injection into the grid to estimate the grid impedance. Additionally, the required complex postprocessing of the measurements is computationally demanding and the real-time implementation of these techniques can be challenging.

This article proposes a novel online event-based grid impedance estimation technique at fundamental frequency relying on PQ variations. The technique consists of combining an accurate active grid impedance estimation technique (PQ variations based on three operating points) with monitoring the PCC voltage magnitude. Under normal operation, the changes in grid impedance will be detected by monitoring the PCC voltage magnitude. The estimation technique will be activated only if a certain change in the voltage magnitude is observed. As a result, PQ variations are performed only in such situations, thus minimizing the power losses and the impact on power quality by avoiding periodic disturbances as in [22]–[27]. The proposed approach is valid for balanced three-phase systems. It offers several advantages:

1) simple algorithm requiring only three samples to perform the estimation of the grid impedance parameters;
2) minimizing the disturbance time;
3) ability to distinguish between various operating scenarios of the inverter to avoid unnecessary PQ variations.

The rest of the article is organized as follows. A detailed description of the proposed technique including the system modeling of the grid-connected inverter is illustrated in Section II. Section III presents the simulation results of the proposed online event-based grid impedance estimation. In Section IV, the experimental validation and results are presented. Finally, the conclusion is summarized in Section V.

## II. Description of Proposed Technique

### A. Inverter System Modeling

The grid-connected inverter system considered in this article is depicted in Fig. 1. The inverter is fed by a constant dc voltage source and connected to the grid through an *LCL* filter. The LV distribution network is modeled by an equivalent Thévenin model, as will be illustrated in the next subsection.

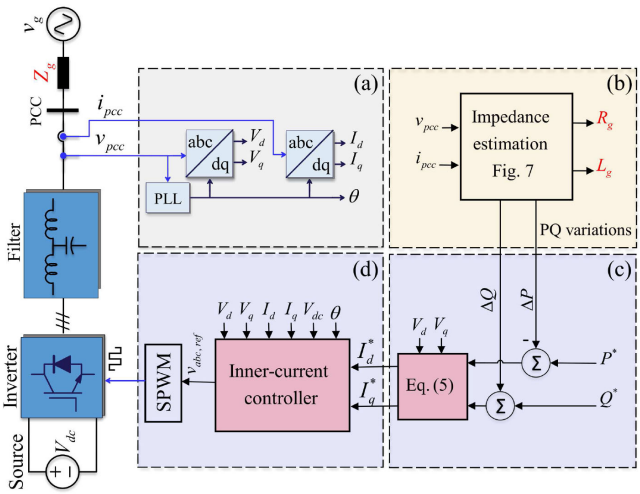


Fig. 1. Simplified diagram of the three-phase grid connected inverter system including the proposed grid impedance estimation technique. (a) Measurements conditioning. (b) Online grid impedance estimation. (c) Current references calculation. (d) Inner-current controller and PWM pulses generation.

The inverter control is implemented in the *dq* reference frame. Moreover, the open-loop power control strategy is used to generate *dq*-current references ($I_d^*,\ I_q^*$). The control loop is modified in order to allow the implementation of the proposed online grid impedance estimation algorithm. For example, the required active and reactive power variations ($\Delta P,\ \Delta Q$) can be added to the power references ($P^*,\ Q^*$).

### B. Equivalent Thévenin Models of Grid Impedance: RL Model Versus RLC Model

The LV distribution network is usually represented by an equivalent Thévenin model. This model is consisting of a grid voltage source ($V_g$) and a grid impedance ($Z_g$). The grid impedance is represented by either the *RL* model ($Z_{g,RL}$) or the *RLC* model ($Z_{g,RLC}$), as shown in (1) and (2), respectively. In the first model, $Z_g$ is represented as series resistance ($R_g$) and inductance ($L_g$). However, the second model includes the equivalent network capacitance seen at the PCC ($C_g$). Therefore, the *RLC* model will have an additional branch ($Z_2 = 1/sC_g$) in parallel with ($Z_1 = R_g + sL_g$) [21], [33]

$$Z_{g,\ RL}(s) = R_g + sL_g \tag{1}$$

$$Z_{g,\ RLC}(s) = Z_1//Z_2 = \frac{R_g + sL_g}{1 + R_gC_gs + L_gC_gs^2}. \tag{2}$$

It is a common practice in the power electronics community to consider the equivalent *RL* model of the utility grid [34]. To further illustrate the differences between the *RL* and *RLC* models, Fig. 2 compares the bode plots for *RL* model and *RLC* models of the grid impedance. In both models, the values of $R_g$ and $L_g$ are listed in Table I. In addition, the value of $C_g$ is set to 0.35 $\mu$F for the *RLC* model. Fig. 2 clearly shows that both the *RL* model and *RLC* model are identical at low frequencies, including 50 Hz. Therefore, the *RL* model is considered in this article as it is sufficient to obtain an accurate representation of

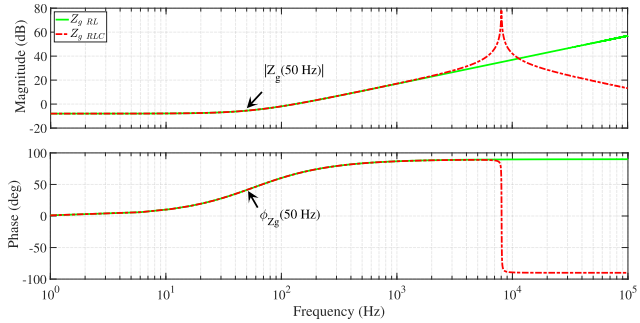


Fig. 2. Equivalent models of grid impedance: *RL* model versus *RLC* model.

TABLE I
SIMULATION PARAMETERS OF THE SYSTEM

| Description | Symbol | Value | Unit |
|---|---|---|---|
| Grid voltage (L-G, MAX) | $V_g$ | $230\sqrt{2}$ | V |
| System angular frequency | $\omega_s$ | $2\pi 50$ | rad/s |
| Grid resistance | $R_g$ | 0.4 | Ω/ km |
| Grid inductance | $L_g$ | $0.35/\omega_s$ | H/km |
| Inverter DC input voltage | $V_{dc}$ | 650 | V |
| Inverter nominal power | $P_n$ | 2.2 | kW |
| Inverter nominal current (L-G, RMS) | $I_n$ | 3.19 | A |
| Inverter-side filter inductance | $L_{f1}$ | 3 | mH |
| Grid-side filter inductance | $L_{f2}$ | 0.6 | mH |
| Filter capacitor | $C_f$ | 4 | $\mu$F |
| Damping resistance | $R_d$ | 3.7 | Ω |
| Switching frequency | $f_{sw}$ | 10 | kHz |
| Sampling frequency | $f_s$ | 10 | kHz |

the grid impedance at the fundamental frequency. Additionally, the subscript $_{RL}$ will be omitted from $Z_{g,\ RL}$ for the rest of this article.

### C. Detection of Grid Impedance Variations by Monitoring the PCC Voltage

In balanced grid operating conditions of the inverter system shown in Fig. 1, the PCC phase voltage vector $\mathbf{V}_{\text{pcc}}$ can be generally expressed as

$$\mathbf{V}_{\text{pcc}} = \mathbf{I}_{\text{pcc}} \times \mathbf{Z}_g + \mathbf{V}_g \tag{3}$$

where $\mathbf{I}_{\text{pcc}}$ and $\mathbf{V}_g$ are inverter output current and grid voltage vectors, respectively. $\mathbf{Z}_g = Z_g\angle\theta_{Z_g}$ is the grid impedance vector of the *RL* model at system frequency ($\omega_s$). Equation (2) reveals that: 1) if $I_{\text{pcc}}$, $V_g$ and $Z_g$ are constant for a certain steady-state operation condition, $V_{\text{pcc}}$ will remain constant; and 2) for a constant value for $V_g$, any change in $V_{\text{pcc}}$ will be caused by either a change in $Z_g$ or $I_{\text{pcc}}$. Therefore, an algorithm for detecting the grid impedance changes based on $V_{\text{pcc}}$ monitoring can be established. It is worth mentioning that this algorithm should distinguish between the various operation scenarios of the inverter. For example, it should be able to identify what caused the change in PCC voltage, and whether it is due to changes in $Z_g$ or in inverter's output current/inverter's P and Q of the inverter itself.

To illustrate how the changes in grid impedance translate into changes in $V_{\text{pcc}}$, let us denote the magnitude of the voltage drop

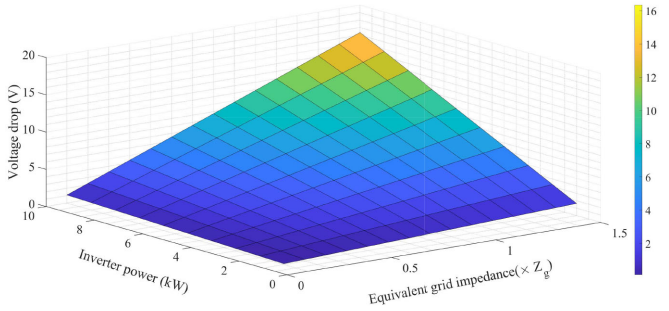


Fig. 3. Voltage drop across the equivalent grid impedance as a function of cable lengths and inverters rated from 1 to 10 kW.

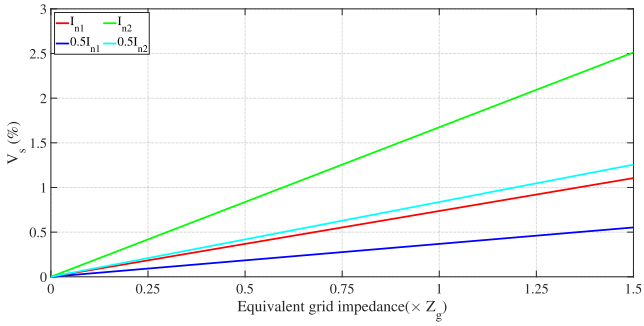


Fig. 4. Voltage sensitivity factor (threshold) as a function of the equivalent grid impedance and the injected currents of two inverters with different rated powers.

across the equivalent grid impedance by $\Delta V_{Z_g} = I_{\text{pcc}} \times Z_g$. By considering the inverter system parameters listed in Table I, Fig. 3 shows the relation between the $\Delta V_{Z_g}$ and the corresponding various grid impedance values ranging [0.1–1.5]$\times Z_g$, where $Z_g = \sqrt{0.4^2 + 0.35^2} = 0.53\ \Omega$. Different case studies are investigated corresponding to inverters with various power ratings ranging 1–10 kW. It can be observed that larger voltage drops are associated with larger values of $Z_g$. Furthermore, the largest voltage drop value is 16.34 V. This value is associated with the 10-kW inverter, where the grid impedance is equal to 1.5 $\times$ $Z_g$. Another example is the voltage drop across the impedance for 2 and 5 kW for 1 $\times$ $Z_g$ is 2.18 and 5.45 V, respectively. It can be concluded from Fig. 3 that each value for $\Delta V_{Z_g}$ corresponds to a specific operating point of the inverter system, which is determined by the inverter output current and grid impedance. Therefore, $\Delta V_{Z_g}$ could be utilized for grid impedance monitoring purposes. It will be seen by the inverter as a change (increase or decrease) in the voltage that is being added to the grid source voltage.

To facilitate easy implementation of the grid voltage monitoring at the PCC, the grid voltage monitoring algorithm could be achieved based on its *dq*-components since the inverter controller is implemented in the *dq* reference frame. Furthermore, it is sufficient to monitor the amplitude of its $d$ component, $V_{\text{pcc}} \cong V_d$. The sensed $q$ component of the voltage ($V_q$) can be neglected since it is regulated to zero by the PI controller of the synchronous reference frame phase-locked loop (SRF-PLL). Hence, $\Delta V_{Z_g}$ can be expressed mathematically in percentage as shown in (4). It is defined as the maximum value of the voltage drop across the equivalent grid impedance ($\Delta V_{Z_g} = I_{\text{pcc}} \times Z_g$) over the amplitude of the nominal phase to ground voltage ($V_{d\ \text{base}} = 230\sqrt{2}$). This term is useful to determine the maximum desired detectable impedance changes based on the monitored PCC voltage magnitude, $V_d$. So, it will be referred to it in the rest of this article as the voltage sensitivity factor ($V_s$), alternatively voltage threshold

$$V_s = \frac{I_{\text{pcc}} \times Z_g}{V_{d\ \text{base}}} \times 100. \tag{4}$$

Fig. 4 shows the relationship between $V_s$ and $Z_g$ for a 2.2 and 5-kW inverter systems denoted by 1 and 2, respectively. Fig. 4 can be used to select appropriate values for $V_s$ to detect

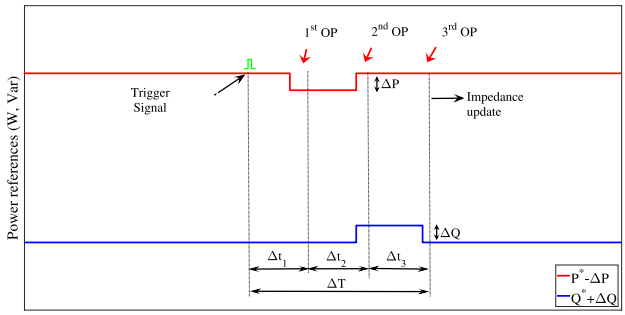


Fig. 5. Proposed event-based variations technique of active and reactive power for grid impedance estimation.

specific impedance changes. For instance, $V_s$ should be set to a value equal or less than 0.74% but not zero in order to detect an impedance change with a resolution of $R_g$= 0.4 $\Omega$ and $L_g = 0.35/\omega_s$ for a 2.2-kW inverter operating at its nominal current ($I_{n1}$). Similarly, $V_s$ should be set to $\leq 0.37\%$ when the inverter injects $0.5 \times I_{n1}$. This allows continuous monitoring of $V_d$ and a trigger signal could be generated once any change in $V_d$ related to $Z_g$ is observed. After that, the trigger signal will activate an online grid impedance estimation technique to obtain accurate information about the new values of the equivalent grid impedance components ($R_g$ and $L_g$).

### *D. Grid Impedance Estimation Using PQ Variations*

Fig. 5 illustrates the proposed event-based PQ variations strategy. The main idea is to intentionally enforce the inverter to work in different operating points throughout deliberate variations in the output active and reactive power [22]. Then, the grid impedance can be extrapolated by avoiding the unknown grid voltage source ($V_g$); see (3). The PQ variations strategy shown in Fig. 5 is based on three operating points, similar to [27]. However, further modifications are considered here including the implementation into a single loop controller in the *dq* reference frame. Furthermore, the proposed technique here has the advantage of avoiding the unnecessary periodic PQ variations compared to what was proposed in [22]–[27]. The PQ variations will be activated only if a trigger command is received. Therefore, it minimizes the required PQ variations.

The motivation behind adapting PQ variations based on three operating points is to minimize the inherent coupling in the *dq* reference frame [27]. This leads to a significant improvement in the impedance accuracy without any need to set the inverter output active power to zero during the estimation process.

The required variations in the active power and reactive power are denoted by $(\Delta P)$ and $(\Delta Q)$, respectively. Then, PQ open-loop power control translates the active and reactive power command signals $(P^* - \Delta P \ \& \ Q^* + \Delta Q)$ into $d$ and $q$ components of the reference current $(I_d^* \ \& \ I_q^*)$, using the following matrix [32]:

$$\begin{bmatrix} I_d^* \\ I_q^* \end{bmatrix} = \frac{2}{3}\frac{1}{V_d^2 + V_q^2}\begin{bmatrix} V_d & -V_q \\ V_q & V_d \end{bmatrix}\begin{bmatrix} P^* - \Delta P \\ Q^* + \Delta Q \end{bmatrix}. \tag{5}$$

Then, the grid impedance is estimated based on sampling three operating points, where $\Delta T$ is the total time required to obtain these three operating points. The procedure of the proposed impedance estimation is summarized as follows.

1) An enable command activates the PQ variations.
2) The first operating point is obtained from the steady-state conditions of the system at $\Delta t_1$, before applying any variations in $P^*$ and $Q^*$.
3) $R_g$ is estimated by considering $\Delta P$ for a specific time $\Delta t_2$ to obtain the second operating point. Then, $R_g$ is calculated from the real part of (6) as shown in (7).
4) $L_g$ is estimated by considering $\Delta Q$ for a specific time $\Delta t_3$ to obtain the third operating point. After that, $L_g$ is calculated from the imaginary part of (6) as shown in (8), where $\Delta t_1 = \Delta t_2 = \Delta t_3 = \frac{\Delta T}{3}$

$$\mathbf{Z}_g^+ = \frac{\Delta \mathbf{V}_{dq}^+}{\Delta \mathbf{I}_{dq}^+} \tag{6}$$

$$R_g^+ = \Re\left[\frac{\Delta \mathbf{V}_{dq}^+}{\Delta \mathbf{I}_{dq}^+}\bigg|_{\Delta P \neq 0,\ \Delta Q = 0}\right] \tag{7}$$

$$L_g^+ = \frac{1}{\omega_s}\Im\left[\frac{\Delta \mathbf{V}_{dq}^+}{\Delta \mathbf{I}_{dq}^+}\bigg|_{\Delta P = 0,\ \Delta Q \neq 0}\right] \tag{8}$$

where $V_d^+, V_q^+, I_d^+$, and $I_q^+$ are the decomposed symmetrical positive-sequences in the *dq* reference frame. The use of positive-sequence components is adopted for reliability reasons, as it will be explained in Section II E. Equation (7) and (8) are expanded further to the folllowing:

$$R_g = \frac{\Delta V_{d12}^+ \times \Delta I_{d12}^+ + \Delta V_{q12}^+ \times \Delta I_{q12}^+}{\Delta {I_{d12}^+}^2 + \Delta {I_{q12}^+}^2} \tag{9}$$

$$L_g = \frac{1}{\omega}\frac{\Delta V_{q13}^+ \times \Delta I_{d13}^+ - \Delta V_{d13}^+ \times \Delta I_{q13}^+}{\Delta {I_{d13}^+}^2 + \Delta {I_{q13}^+}^2}. \tag{10}$$

### *E. Proposed Online Even-Based Grid Impedance Estimation Technique*

Fig. 6 shows the detailed flow chart of the proposed event-based online grid impedance estimation technique. Moreover, Fig. 7 gives further explanation on the online implementation.

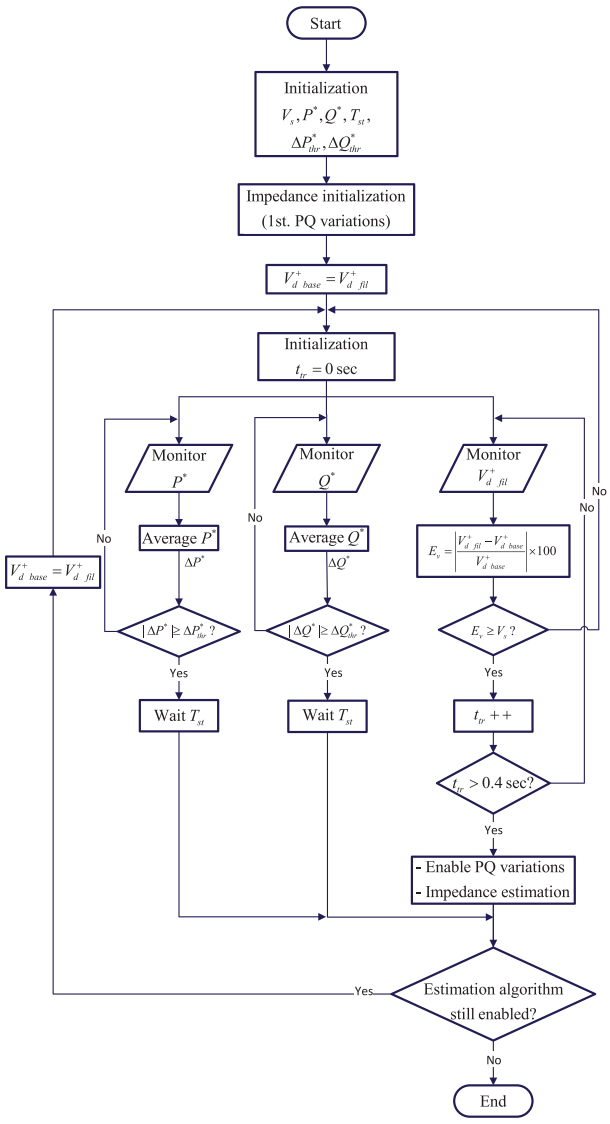


Fig. 6. Flow chart of the proposed algorithm for event-based grid impedance estimation technique.

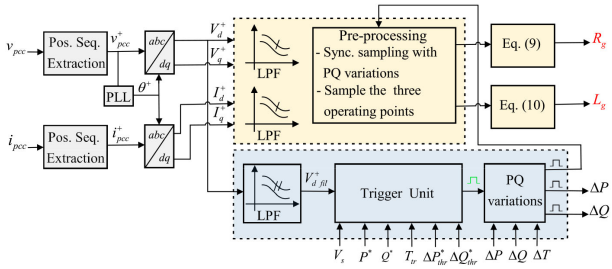


Fig. 7. Proposed methodology for online grid impedance estimation.

Once the algorithm starts, the PQ variations will be enabled immediately to allow initialization of the impedance parameters. Then, any detection of change in the grid voltage amplitude exceeding the predefined conditions, i.e., of $V_s$, will be used to trigger the PQ variations technique again. Monitoring of the grid voltage amplitude is achieved based on the *d*-component of the positive-sequence, $V_d^+$. This is to ensure the monitoring

process is achieved based on balanced components even if the original grid voltage is unbalanced [17]. Then, this voltage is properly filtered ($V^+_{d\,\text{fil}}$) using a low pass filter (LPF) with a desired settling time ($T_{st}$) before it is sent to the trigger unit for continuous monitoring purposes. Then, the absolute percentage error in the voltage amplitude, denoted by $E_v$, is calculated with respect to its initial value ($V^+_{d\,\text{base}}$). After that, the trigger unit used the error information to make a decision whether to enable the PQ variations again to estimate the grid impedance or not.

In more details, the trigger unit works as follows. It continuously checks three conditions and compares them to their thresholds in order to decide the cause of the PCC voltage magnitude rise/drop. These conditions are the variation of active power reference ($\Delta P^*$), the variation of the reactive power reference ($\Delta Q^*$), and the error $E_v$. $\Delta P^*$ and $\Delta Q^*$ are averaged over a 5-Hz window, where their current values are compared to the previous values to detect any changes in their values. After that, the detected absolute $\Delta P^*$ and $\Delta Q^*$ will be compared to predefined thresholds ($\Delta P^*_{\text{thr}}$ and $\Delta Q^*_{\text{thr}}$) greater than zero. If any of these two (or both) conditions are satisfied, the estimation algorithm will not be activated to avoid unnecessary PQ variations. However, $V^+_{d\,\text{base}}$ value will be updated to $V^+_{d\,\text{fil}}$. If any change in $E_v$ is detected and it is bigger than the threshold value $V_s$, a timer is activated. The time value of the timer is named $t_{tr}$ and its initial condition is set to 0 s. If $E_v$ remains larger than the threshold value for more than $t_{tr}$, a trigger signal is sent to enable the PQ variations and $V^+_{d\,\text{base}}$ value will be updated to $V^+_{d\,\text{fil}}$. Otherwise, if $E_v$ does not exceed the threshold value within $t_{tr}$, the timer is reset to 0 s.

$V_s$ can be chosen to a wide range of values, but it should be within the desired resolution of the grid impedance to be detected. It is worth mentioning that the timer value is chosen here to $t_{tr}$= 0.4 s since we target the steady operation of the inverter and to avoid any short-term grid transients.

## III. Simulation Results

A three-phase three-wire inverter system based on the discrete-time model is simulated using MATLAB/Simulink environment and PLECS toolbox components. The simulated inverter system is shown in Fig. 1. The system parameters are listed in Table I. Three case studies are investigated to demonstrate the performance of the proposed event-based online grid impedance estimation technique. The first case study compares the proposed technique with the conventional PQ variations technique. The second case study examines the performance of the proposed technique as a function to different realistic $R/X$ ratios for the LV distribution networks. Finally, the third simulated case study looks into effects of the impedance of other converters, located close to the inverter estimating the grid impedance.

### *A. Comparison Between the Proposed and the Conventional Techniques for Online Grid Impedance Estimation*

The sequence of the simulated events is as follows. Firstly, at 0 s: The inverter starts by injecting only active power at 2.2 kW and the grid impedance parameters are set to $R_g = 0.8\ \Omega$ and $L_g =$ 2.22 mH, double of the impedance parameters' values presented in Table I. Secondly, at 0.6 s: The grid impedance estimation algorithm is enabled. The algorithm initialization parameters are set to $P^* = P_n = 2.2$ kW, $Q^* = 0$ Var, $V_s = 0.3\%$, $V^+_{d\,\text{base}} = 230\sqrt{2}$ V, $T_{st} = 0.1$ s, $t_{tr} = 0.4$ s, $\Delta P = \Delta Q = 20\% P_n$ , $\Delta T =$ 0.3 s, $\Delta P^*_{\text{thr}} = 5$ W, $\Delta Q^*_{\text{thr}} = 5$ Var. Thirdly, at 3 s: The impedance components are reduced to $R_g = 0.4\ \Omega$ and $L_g = 1.11$ mH, half of its previous value. $V_s = 0.3\%$ is sufficient to detect the impedance changes with a resolution of $R_g = 0.4\ \Omega$ and $L_g = 1.11$ mH, when the inverter injects current within the range $I_n/2 \leq I \leq I_n$ as illustrated previously in Fig. 4. Fourth, at 4.5 s: The active power reference is reduced to $P^* = 0.8$ kW.

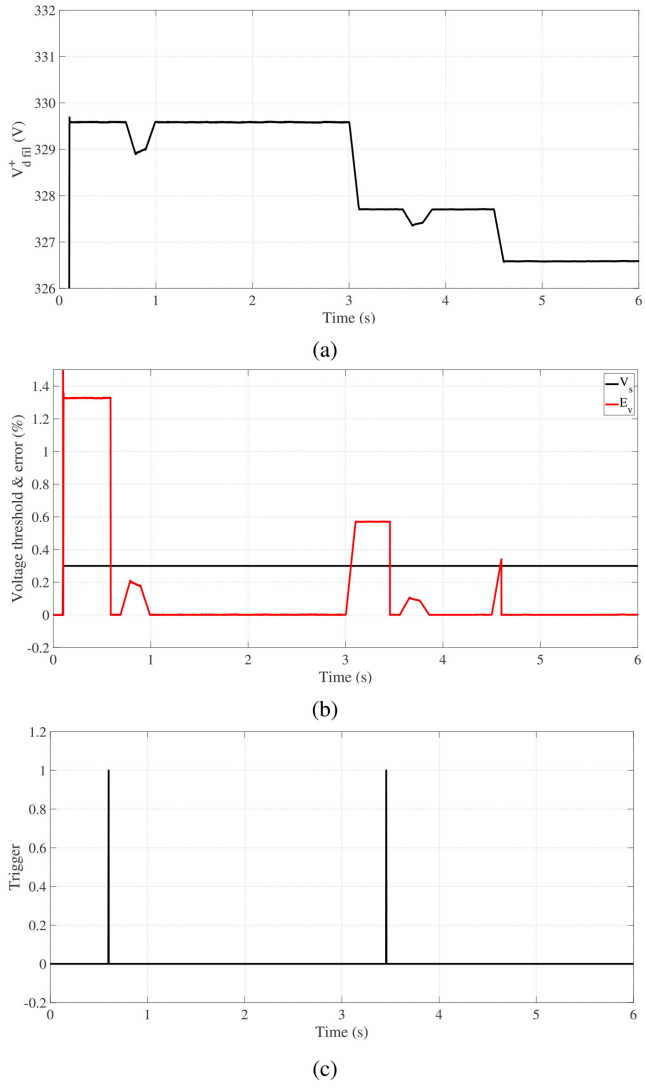


Fig. 8. Simulation results of the proposed estimation algorithm when the inverter injects only active power. (a) Monitored grid voltage magnitude. (b) Voltage threshold and error signals. (c) Trigger command.

Fig. 8(a) shows $V^+_{d\,\text{fil}}$ with $T_{st}$= 0.1 s. $V^+_{d\,\text{fil}}$ reaches 329.6 V at 0.1 s, then it was reduced to 327.7 and to 326.6 V corresponding to $\mathbf{Z}_g$ and $P^*$ changes at 3 and 4.5 s, respectively. Fig. 8(b) compares the constant threshold $V_s$ with the instantaneous error to generate a trigger once the preset conditions are satisfied. At 0.1 s, $E_v$ is 1.33% due to the difference between the initial

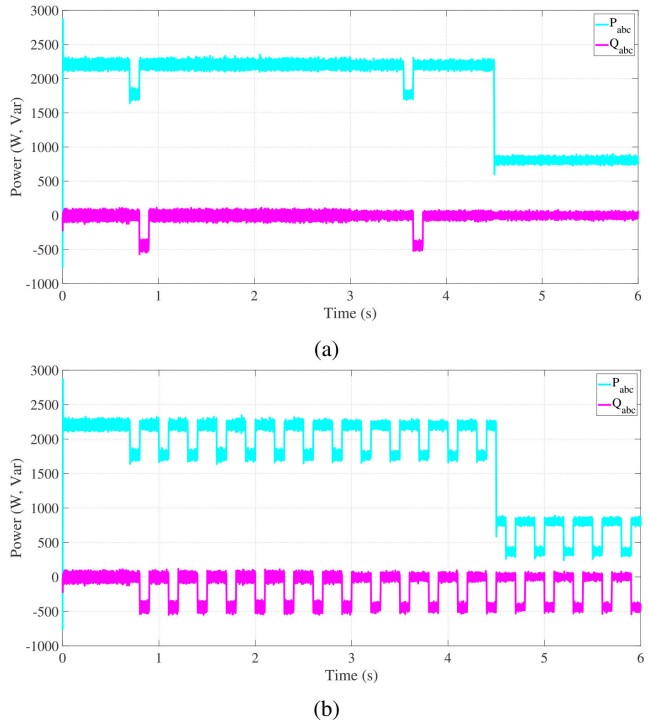


Fig. 9. Delivered power at the PCC. (a) Proposed even-based PQ variations techniques. (b) Conventional periodic PQ variations.

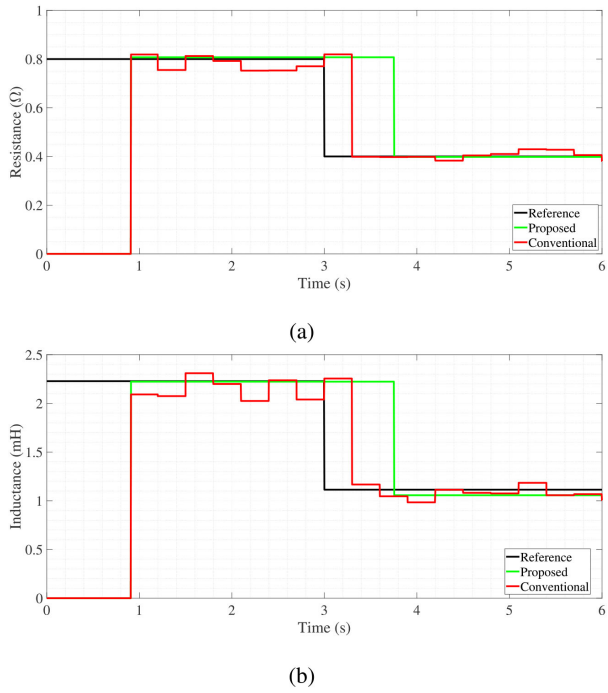


Fig. 10. Comparison between the proposed and the conventional periodic PQ variations techniques. (a) Grid resistance. (b) Grid inductance.

$V_{d\,\text{base}}^{+} = 325.2$ V and the measured $V_{d\,\text{fil}}^{+} = 329.6$ V. Once the grid impedance algorithm starts at 0.6 s, $V_{d\,\text{base}}^{+}$ value is updated as illustrated in Fig. 6. Consequently, the $E_v$ is reset to zero. Similarly, these values are updated at 3.45 and 4.6 s. $\mathbf{Z}_g$ estimation algorithm is enabled two times, at 0.6 and 3.45 s, as shown in Fig. 8(c). At each time the PQ variations are enabled, $V_{d\,\text{base}}^{+}$ will be updated simultaneously.

Fig. 9(a) shows the inverter's output power when the proposed grid impedance technique is activated at 0.6 s. $\Delta P$ and $\Delta Q$ are applied from 0.7 and 0.8 s, each for 0.1 s; these variations are necessary to obtain the second and third operating points, respectively. The other PQ variations are applied at 3.55 and 3.65 s. On the other hand, Fig. 9(b) shows the periodic variations technique (conventional) based on [27] for the same test conditions. Similarly, all previous studies followed only the periodic PQ variations for the grid impedance estimation purposes [22]–[26]. Fig. 9 shows the superiority of the proposed method. It significantly reduces unnecessary frequent PQ variations. This is important especially in multiinverter systems, where the continuous oscillation of output power of parallel inverters could lead to power quality issues.

Fig. 10 compares the estimated grid impedance from both proposed event-based PQ variations and the periodic PQ variations techniques for the same test conditions. In both techniques, the grid impedance components (resistance and inductance) values were updated for the first time at 0.9 s with small estimation errors with respect to the references. Then, the grid impedance was updated once only at 3.75 s using the proposed technique. In contrast, $\mathbf{Z}_g$ components values were continuously updated each 0.3 s using the conventional technique. Fig. 10 confirms that the proposed technique detected the impedance changes around 0.45 s later than the conventional technique. This time delay is required for the trigger unit to verify the impedance changes, see Fig. 6. As a result, the proposed technique has the advantages of avoiding unnecessary continuous PQ variations and impedance estimation each 0.3 s compared to the conventional technique.

TABLE II
INVESTIGATED $R/X$ RATIOS

| No. | R ($\Omega/km$) | X ($\Omega/km$) | $R/X$ ratio |
|---|---|---|---|
| $Z_1$ | 0.868 | 0.092 | 9.435 |
| $Z_2$ | 0.469 | 0.075 | 6.253 |

### *B. Performance of the Proposed Technique for Different $R/X$ Ratios for the Low Voltage Network*

Typical LV distribution networks are characterized by their high $R/X$ ratios. Therefore, different realistic values of $R/X$ ratios are considered in this case study. The investigated $R/X$ ratios are listed in Table II, where the values are obtained from the European Low Voltage Test Feeder benchmark [35].

The sequence of the simulated events is similar to the previous case study. Fig. 11 compares the constant threshold $V_s$ with the instantaneous measured errors obtained for the $R/X$ ratios of 9.43 and 6.25, respectively. For both $R/X$ ratios, the trigger signals were generated successfully at the moment of enabling the estimation algorithm and when the impedance changes are confirmed. Additionally, Fig. 11 reveals that more voltage drop was associated with the larger $R/X$ ratio.

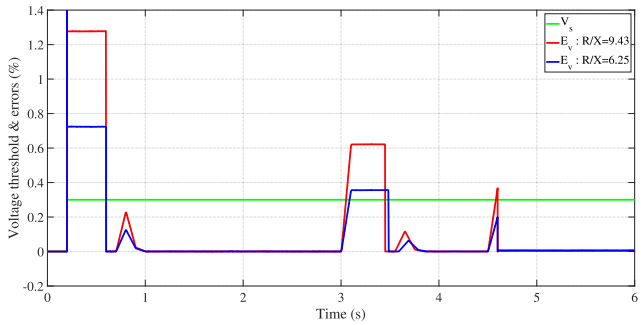


Fig. 11. Simulation results for two different $R/X$ ratios. Voltage threshold and voltage error signals.

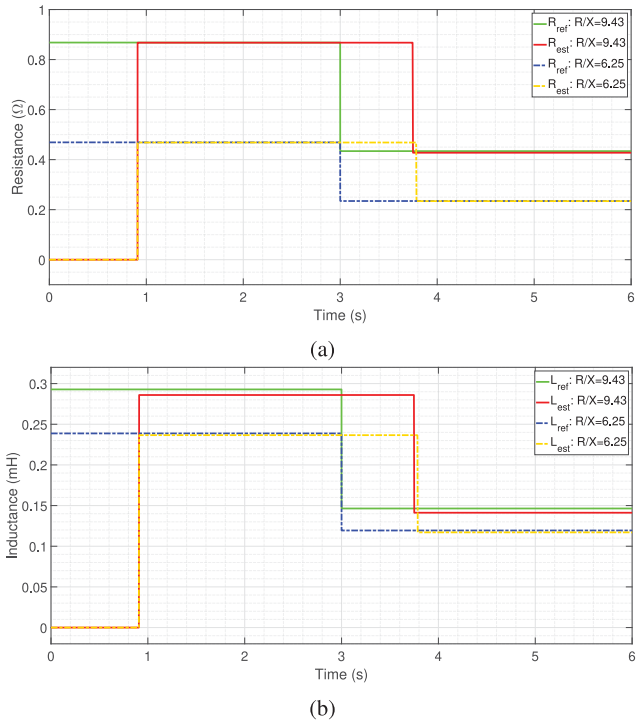


Fig. 12. Comparison of the estimated impedance components using the proposed technique for two different $R/X$ ratios. (a) Grid resistance. (b) Grid inductance.

Fig. 12(a) and (b) shows the estimated resistance and inductance of grid impedance, respectively. Overall, the proposed technique provides very good estimation results for both $R/X$ ratios. Nevertheless, the obtained results are slightly less accurate for the case of the larger $R/X$ ratio, especially the inductive component. This is due to the associated larger coupling between P and Q powers in LV networks due to their larger $R/X$ ratios [36].

### C. Performance Evaluation in Multiple Grid-Connected Inverters

This subsection examines the effects on the impedance at fundamental frequency in the presence of another inverter, located close to the inverter estimating the grid impedance. Two

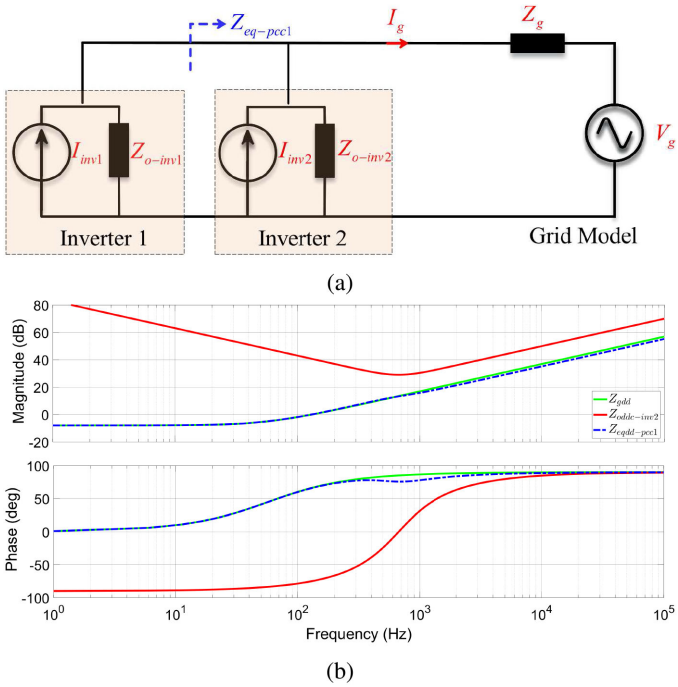


Fig. 13. (a) Equivalent impedance model of two parallel grid-connected inverters operating in current mode. (b) Bode plot of the impedances at *d*-axis.

parallel grid-connected inverters operating in current mode are considered. Fig. 13(a) shows the network impedance model based on Norton equivalent circuit of the inverters. Therefore, the equivalent impedance seen by the inverter 1 ($Z_{eq-\text{pcc1}}$) will be the parallel connection of impedances $Z_g$ and $Z_{o-\text{inv2}}$, where $Z_{o-\text{inv2}}$ is the output impedance of inverter 2. The value of grid impedance dominates the equivalent impedance at low frequencies since $Z_g \ll Z_{o-\text{inv2}}$.

Fig. 13(b) shows the bode plot of the analytical impedances in the *d*-axis. The plotted impedances at *d*-axis are the grid impedance ($Z_{\text{gdd}}$), the output impedance of inverter 2 ($Z_{\text{oddc}-\text{inv2}}$) and the equivalent network impedance seen by inverter 1 ($Z_{\text{eqdd}-\text{pcc1}}$). Inverter 2 is interfaced to the utility grid through an *L*-filter and it operates in unity power factor, where its rated power is 5 kW. And $Z_{\text{oddc}-\text{inv2}}$ is presented in [37]. Fig. 13(b) shows that both the equivalent network seen by inverter 1 and the grid impedance are identical at 50 Hz, $Z_{\text{eqdd}-\text{pcc1}}(50\text{ Hz}) \cong Z_{\text{gdd}}(50\text{ Hz})$. Hence, the *RL* model of the grid impedance at the fundamental frequency is valid and provides very accurate results even in the presence of other nearby inverters.

## IV. Experimental Results

Fig. 14 shows the experimental test setup. The control algorithm was implemented using MATLAB/Simulink and then built to dSPACE 1103 controller board. A three-phase inverter rated at 2.2 kW was used. It was supplied by a 650 V dc voltage source. The inverter was interfaced with the grid through an *LC* filter, $L_f = 1.8$ mH and $C_f = 4.7$ $\mu$F. Moreover, the inverter was connected to the LV network (230 V and 50 Hz) through a 5-kVA

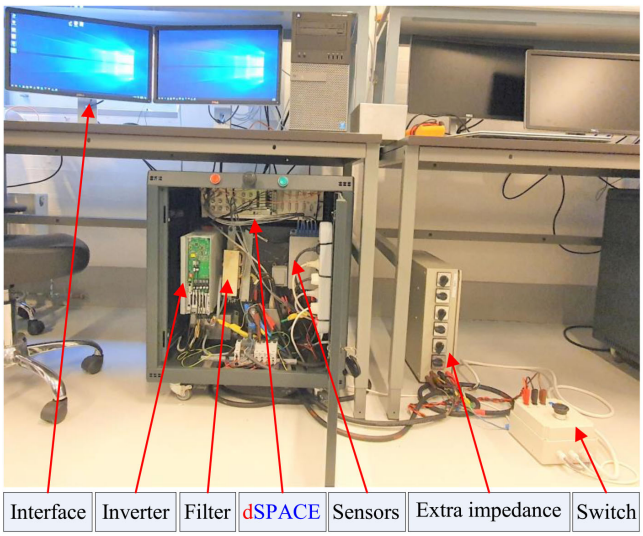


Fig. 14. Experimental test setup used for testing the proposed technique of online event-based grid impedance estimation.

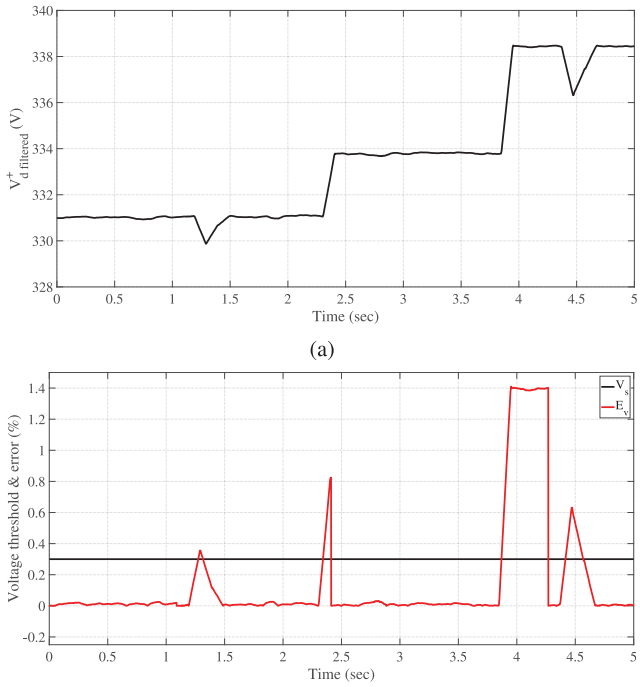


Fig. 15. Experimental results when the inverter injects active power. (a) Monitored grid voltage. (b) Voltage threshold and error signals.

isolation transformer with a leakage inductance of 1.5 mH and resistance of 0.3 Ω. In addition, an extra impedance consisting of a resistance and an inductance with values of 1 Ω and 2 mH was used to test the grid impedance variations.

The extra impedance was inserted in series between the PCC and the isolation transformer using a switch. The switch was manually controlled to allow the extra impedance to be added after a certain time. Several case studies were investigated. In all case studies, the proposed algorithm was tested for the impedance jump from $R_{\text{ref1}} = 1.5\,\Omega$ and $L_{\text{ref1}} = 1.5$ mH, without the additional impedance, to $R_{\text{ref2}} = 2.5\,\Omega$ and $L_{\text{ref2}} = 3.5$ mH, with the additional impedance.

The rationale for choosing the value of the additional impedance for the experimental tests was to maintain a significant ratio of change with respect to initial values. This was a limitation of the existent experimental setup, where the scale down 5-kVA distribution transformer resulted in a significantly larger leakage inductance which dominates the grid impedance, unlike realistic low voltage distribution networks (LVDNs) where the distribution transformers are typically rated higher than 50 kVA and up to 500–1000 kVA, which results in a significantly smaller leakage inductance.

The first case study considered a jump in active power reference and grid impedance, respectively. Fig. 15(a) shows the monitored $V^+_{d\,\text{fil}}$. Initially, its value was around $V^+_{d\,\text{fil}} = 331$ V when the inverter injected only active power at $P^* = 1$ kW. This value is changed to $V^+_{d\,\text{fil}} = 333.7$ V and to $V^+_{d\,\text{fil}} = 338.5$ V. The last two changes in the grid voltage amplitude are corresponding to the change in the active power reference to $P^* = 2$ kW and to the inserted additional impedance using the manual switch, respectively. The threshold $V_s = 0.3\%$ is continuously compared with $E_v$, as shown Fig. 15(b). The error exceeded the threshold four times. Two times, the first and fourth times, were temporary fluctuations due to the deliberate PQ variations required for impedance estimation. The other two occasions are due to the change in $P^*$ and $\mathbf{Z}_g$ at 2.29 and 3.84 s, respectively. The estimation algorithm is able to distinguish these different cases and only triggers the PQ variations at 4.27 s, besides the first one at 1.09 s to find the initial value of the impedance.

Fig. 16 shows results in ControlDesk for the grid impedance estimation. The first values of the grid impedance parameters are obtained at 1.39 s, after the estimation algorithm is activated at 1.09 s. $R_{\text{est1}} = 1.40\,\Omega$ and $L_{\text{est1}} = 1.49$ mH. These values are updated to $R_{\text{est2}} = 2.51\,\Omega$ and $L_{\text{est2}} = 3.51$ mH at 4.57 s. Fig. 16 also shows $P^*$ and $Q^*$.

Another case study experimentally tested is shown in Fig. 17. It represents the activation of grid impedance estimation algorithm when there is no power flow between the inverter and the grid. The estimation algorithm is activated at 1.316 s. Then, the inverter starts absorbing reactive power $Q^* = 1$ kVar at $t = 2.6$ s. Finally, an impedance jump is applied at 3.91 s. Fig. 17(a) and (b) show the inverter output current and the monitored $V^+_{d\,\text{fil}}$, respectively. Fig. 18 shows the results in ControlDesk for the online estimated grid impedance. The first set of the estimation results is obtained at 1.62 s, where $R_{\text{est1}} = 1.42\,\Omega$ and $L_{\text{est1}} = 1.47$ mH. These values are updated to $R_{\text{est2}} = 2.56\,\Omega$ and $L_{\text{est2}} = 3.96$ mH at 4.64 s. This is evident that the proposed grid impedance estimation algorithm is reliable, where it has the ability to initialize the grid impedance values immediately after the estimation algorithm is activated, even without power flow between the inverter and the grid. The application of grid impedance measurements in such operating scenario could be, for example, the adaptive control tuning of grid-connected inverter during start-up.

Table III summarizes the above-investigated tests, named Test 1 and Test 2, respectively. Two additional tests considering other

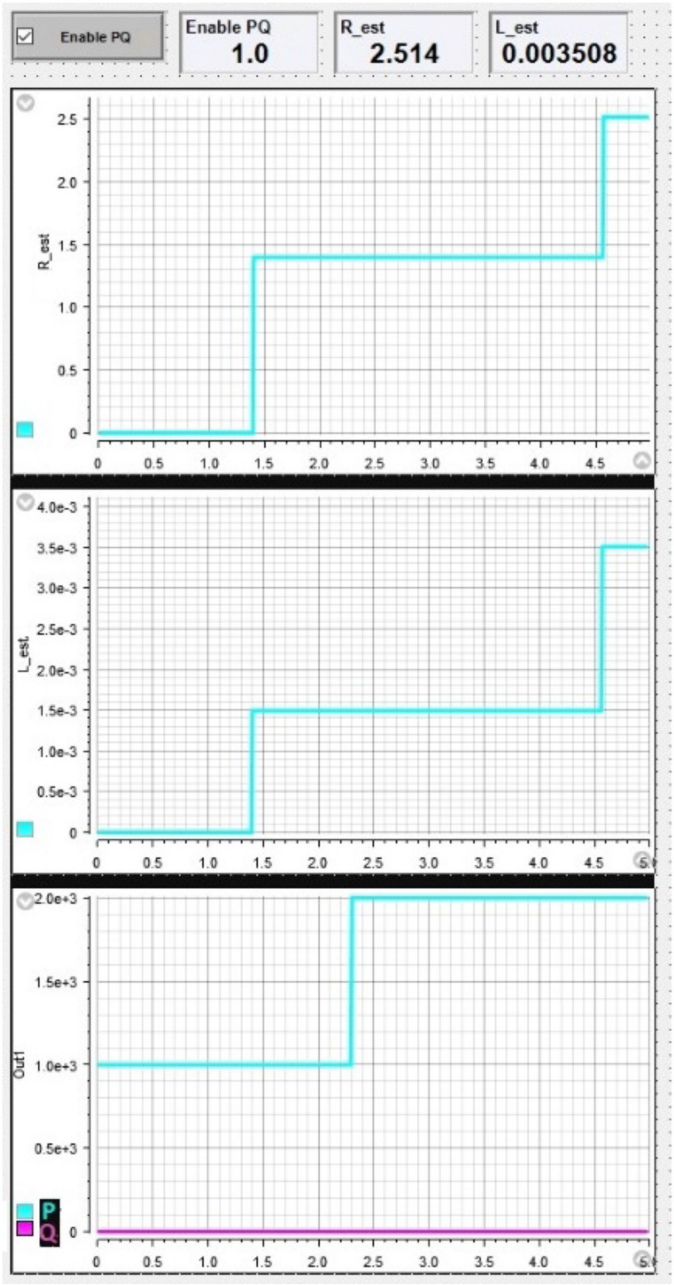


Fig. 16. ControlDesk interface displays the experimental results when the inverter injects active power. (Top) The estimated grid resistance (Ω). (Middle) The estimated grid inductance (H). (Bottom) The inverter power references, $P^*$ and $Q^*$, (W, Var).

TABLE III
EXPERIMENTAL RESULTS OF ONLINE IMPEDANCE ESTIMATION FOR DIFFERENT TESTED OPERATING CONDITIONS OF THE INVERTER

| Test No. | Tested parameters | $R_{est1}$ (Ω) | $L_{est1}$ (mH) | $R_{est2}$ (Ω) | $L_{est2}$ (mH) |
|---|---|---|---|---|---|
| Test 1 | $P_1^*$= 1 kW, $P_2^*$= 2 kW, $Q^*$= 0 kVar | 1.40 | 1.49 | 2.51 | 3.51 |
| Test 2 | $Q_1^*$= 0 kVar, $Q_2^*$= -1 kVar $P^*$= 0 kW | 1.42 | 1.47 | 2.56 | 3.96 |
| Test 3 | $P^*$= 1.5 kW, $Q^*$= +1 kVar | 1.33 | 1.25 | 2.52 | 3.49 |
| Test 4 | $P^*$= 1.5 kW, $Q^*$= -1 kVar | 1.35 | 1.41 | 2.56 | 3.71 |

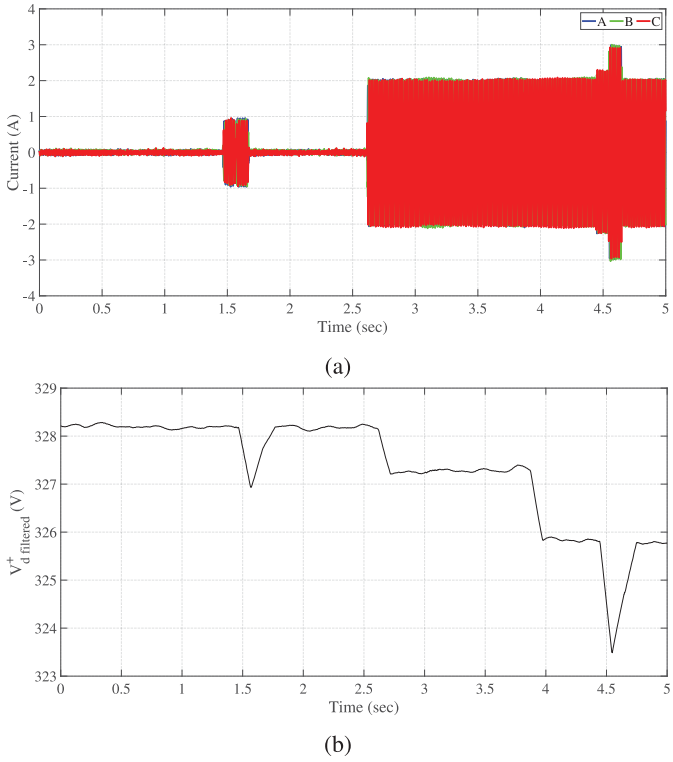


Fig. 17. Experimental results when the inverter only absorbs reactive power. (a) Inverter output current. (b) Monitored grid voltage.

operating scenarios of the grid-connected inverter system are also reported. These include the injection of active power and injection/absorption of reactive power; see test 3 and test 4, respectively. In each of these tests, the equivalent grid impedance components changes from $R_{\text{ref1}} = 1.5\ \Omega$ & $L_{\text{ref1}} = 1.5$ mH to $R_{\text{ref2}} = 2.5\ \Omega$ & $L_{\text{ref2}} = 3.5$ mH. Results validate that the proposed technique successfully updates the impedance values only after impedance changes occurred.

The results presented in Table III also indicate that the errors in both the resistive and inductive components are slightly larger for the last two case studies, Test 3 and Test 4. These two case studies are associated with the nonunity power factor operation of the inverter, which represent extreme and unrealistic operating modes of grid-connected inverters $Q^* = \pm 45\%$ of the inverter rated power. The increase in the estimation errors is explained from the inherent coupling in the *dq* reference frame between the active and reactive powers. The effect of this coupling is well known in the literature, which also poses challenges to accurate control of active and reactive powers especially in LV with high $R/X$ ratios [36]. It is important to point out that the proposed technique enables the inverter to estimate the grid impedance even in standby mode, e.g., Test 2. This makes the proposed technique more reliable compared to the observer-based method [30], which requires power flow in order to obtain the grid impedance using RLS.

It is worth mentioning that the technique proposed in this article is limited to grid impedance estimation at the fundamental frequency only. While the proposed technique estimates the grid

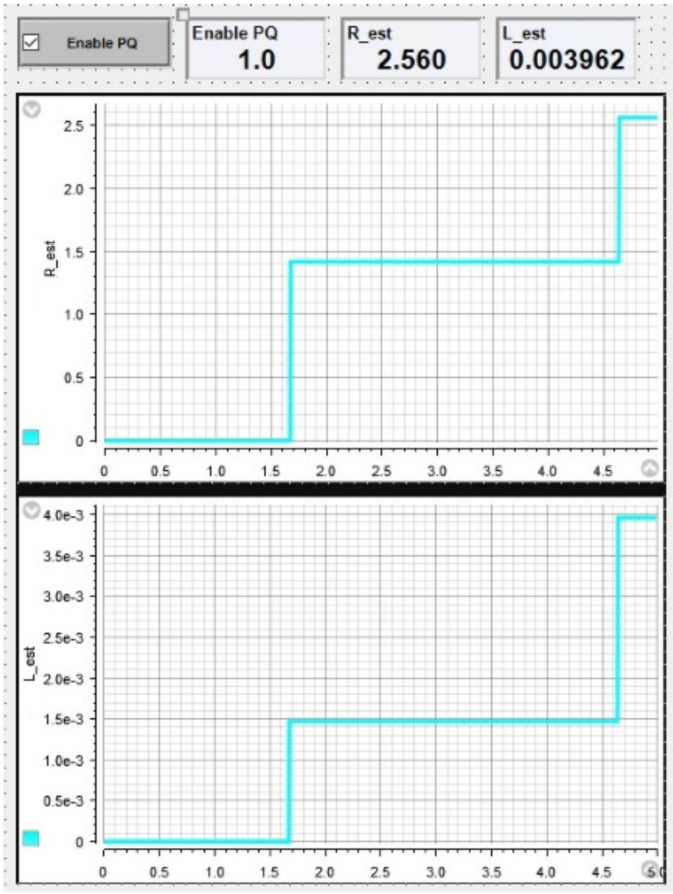


Fig. 18. ControlDesk interface displays the estimated impedance when the inverter only absorbs reactive power. (Top) The estimated grid resistance (Ω). (Bottom) The estimated grid inductance (H).

impedance online, it requires a certain time frame to be used for the trigger unit and the active and reactive power variations. Therefore, some suitable applications for the proposed technique include: voltage control, reactive power support, decoupling the inner current control, and adaptive tuning adaptive controller tuning for grid-connected inverters based on gain scheduling.

## V. Conclusion

This article proposed an online event-based estimation technique to estimate the equivalent grid impedance of balanced three-phase systems at the PCC of the inverter. The estimation technique is embedded into the control loop of a three-phase grid-connected inverter. It is based on a combination of continuous monitoring of the positive-sequence amplitude of the grid voltage and PQ variations technique. Once a change in the voltage amplitude that is related to impedance changes is detected, a trigger signal will be generated and sent to enable the PQ variations technique to accurately estimate the new grid impedance value. Results show that the proposed grid impedance technique significantly reduces the required PQ variations. Apart from that, the proposed technique offers the advantage of being able to estimate the grid impedance values immediately after the estimation algorithm is activated, even if there is no power flow between the inverter and the grid. The performance comparison between the proposed grid impedance estimation technique and a conventional periodic PQ variations is also presented. Both simulation and experimental results are provided to validate and confirm the effectiveness of the proposed estimation technique.

## References

[1] A. P. Sakis Meliopoulos *et al.*, "Smart grid technologies for autonomous operation and control," *IEEE Trans. Smart Grid*, vol. 2, no. 1, pp. 1–10, Mar. 2011.

[2] R. Tonkoski, L. A. C. Lopes, and T. H. M. El-Fouly, "Coordinated active power curtailment of grid connected PV inverters for overvoltage prevention," *IEEE Trans. Sustain. Energy*, vol. 2, no. 2, pp. 139–147, Apr. 2011.

[3] F. Ji, Y. Li, J. Xiang, and S. Liu, "Islanding detection method based on system identification, *IET Power Electron.*, vol. 9, no. 10, pp. 2095–2102, Aug. 2016.

[4] J. De Kooning, J. Van de Vyver, J. D. M. De Kooning, T. L. Vandoorn, and L. Vandevelde, "Grid voltage control with distributed generation using online grid impedance estimation," *Sustain. Energy, Grids Netw.*, vol. 5, pp. 70–77, 2016.

[5] H. Alenius, R. Luhtala, T. Messo, and T. Roinila, "Autonomous reactive power support for smart photovoltaic inverter based on real-time grid-impedance measurements of a weak grid," *Electr. Power Syst. Res.*, vol. 182, Jan. 2020, Art. no. 106207.

[6] A. Vijayakumari, A. T. Devarajan, and N. Devarajan, "Decoupled control of grid connected inverter with dynamic online grid impedance measurements for micro grid applications," *Int. J. Electr. Power Energy Syst.*, vol. 68, pp. 1–14, 2015.

[7] M. Cespedes and J. Sun, "Adaptive control of grid-connected inverters based on online grid impedance measurements," *IEEE Trans. Sustain. Energy*, vol. 5, no. 2, pp. 516–523, Apr. 2014.

[8] T. Roinila, T. Messo, T. Suntio, and M. Vilkko, "Pseudo-random sequences in DQ-domain analysis of feedforward control in grid-connected inverters," *IFAC-PapersOnLine*, vol. 48, no. 28, pp. 1301–1306, 2015.

[9] A. Riccobono *et al.*, Stability of shipboard DC power distribution, *IEEE Electrif. Mag.*, vol. 5, no. 3, pp. 55–67, Sep. 2017.

[10] K. Jia, T. Bi, B. Liu, E. Christopher, D. W. P. Thomas, and M. Sumner, "Marine power distribution system fault location using a portable injection unit," *IEEE Trans. Power Del.*, vol. 30, no. 2, pp. 818–826, Apr. 2015.

[11] D. Babazadeh, A. Muthukrishnan, P. Mitra, T. Larsson, and L. Nordström, "Real-time estimation of AC-grid short circuit capacity for HVDC control application," *IET Gener. Transmiss. Distrib.*, vol. 11, no. 4, pp. 838–846, Mar. 2017.

[12] J. Sun, "Impedance-based stability criterion for grid-connected inverters," *IEEE Trans. Power Electron.*, vol. 26, no. 11, pp. 3075–3078, Nov. 2011.

[13] A. A. A. Radwan and Y. A. R. I. Mohamed, "Modeling, analysis, and stabilization of converter-fed AC microgrids with high penetration of converter-interfaced loads," *IEEE Trans. Smart Grid*, vol. 3, no. 3, pp. 1213–1225, Sep. 2012.

[14] M. Cespedes and J. Sun, "Impedance modeling and analysis of grid-connected voltage-source converters," *IEEE Trans. Power Electron.*, vol. 29, no. 3, pp. 1254–1261, Mar. 2014.

[15] M. Ciobotaru, V. Agelidis, and R. Teodorescu, "Line impedance estimation using model based identification technique," in *Proc. 14th Eur. Conf. Power Electron. Appl.*, 2020, Art. no. 106207.

[16] N. Hoffmann and F. W. Fuchs, "Minimal invasive equivalent grid impedance estimation in inductive resistive power networks using extended Kalman filter," *IEEE Trans. Power Electron.*, vol. 29, no. 2, pp. 631–641, Feb. 2014.

[17] S. Cobreces, E. J. Bueno, D. Pizarro, F. J. Rodriguez, and F. Huerta, "Grid impedance monitoring system for distributed power generation electronic interfaces," *IEEE Trans. Instrum. Meas.*, vol. 58, no. 9, pp. 3112–3121, Sep. 2009, pp. 3112–3121.

[18] L. M. Phuong, H. V. D. Duy, ham T. X. Hoa, and N. M. Huy, "New adaptive droop control with combined line impedance estimation method for parallel inverters," *Sci. Technol. Develop. J.*, vol. 19, no. 4, pp. 45–64, 2016.

[19] M. Ciobotaru, R. Teodorescu, and F. Blaabjerg, "On-line grid impedance estimation based on harmonic injection for grid-connected PV inverter," in *Proc. IEEE Int. Symp. Ind. Electron.*, 2007, pp. 2437–2442.

[20] M. Sumner, B. Palethorpe, D. W. P. Thomas, P. Zanchetta, and M. C. Di Piazza, "A technique for power supply harmonic impedance using a controlled voltage disturbance," *IEEE Trans. Power Electron.*, vol. 17, no. 2, pp. 207–215, Mar. 2002.
[21] A. Riccobono, E. Liegmann, A. Monti, F. Castelli Dezza, J. Siegers, and E. Santi, "Online wideband identification of three-phase AC power grid impedances using an existing grid-tied power electronic inverter," *IEEE 17th Work. Control Model. Power Electron.*, 2016, pp. 1–8.
[22] M. Ciobotaru, R. Teodorescu, P. Rodriguez, A. Timbus, and F. Blaabjerg, "Online grid impedance estimation for single-phase grid-connected systems using PQ variations," in *Proc. IEEE Annu. Power Electron. Specialist Conf.*, no. 1, 2007, pp. 2306–2312.
[23] A. V. Timbus, P. Rodriguez, R. Teodorescu, and M. Ciobotaru, "Line impedance estimation using active and reactive power variations," in *Proc. IEEE Power Electron. Spec. Conf.*, 2007, pp. 1273–1279.
[24] A. V. Timbus, R. Teodorescu, and P. Rodriguez, "Grid impedance identification based on active power variations and grid voltage control," in *Proc. IEEE Ind. Appl. Annu. Meet.*, 2007, pp. 949–954.
[25] L. Wang, J. Chen, X. Li, X. Sun, and J. M. Guerrero, "Fundamental impedance identification method for grid-connected voltage source inverters," *IET Power Electron.*, vol. 7, no. 5, pp. 1099–1105, 2014.
[26] J. H. Cho, K. Y. Choi, Y. W. Kim, and R. Y. Kim, "A novel P-Q variations method using a decoupled injection of reference currents for a precise estimation of grid impedance," in *Proc. IEEE Energy Convers. Congr. Expo.*, Nov. 2014, pp. 5059–5064.
[27] N. Mohammed, M. Ciobotaru, and G. Town, "An improved grid impedance estimation technique under unbalanced voltage conditions," in *Proc. IEEE PES Innov. Smart Grid Technol. Eur.*, 2019, pp. 1–5.
[28] L. A. Maccari, C. L. do A. Santini, H. Pinheiro, R. C. L. F. de Oliveira, and V. F. Montagner, "Robust optimal current control for grid-connected three-phase pulse-width modulated converters," *IET Power Electron.*, vol. 8, no. 8, pp. 1490–1499, 2015.
[29] L. Jessen, S. Gunter, F. W. Fuchs, M. Gottschalk, and H. J. Hinrichs, "Measurement results and performance analysis of the grid impedance in different low voltage grids for a wide frequency band to support grid integration of renewables," in *Proc. IEEE Energy Convers. Congr. Expo.*, 2015, pp. 1960–1967.
[30] P. Garcia, M. Sumner, A. Navarro-Rodriguez, J. M. Guerrero, and J. Garcia, "Observer-based pulsed signal injection for grid impedance estimation in three-phase systems," *IEEE Trans. Ind. Electron.*, vol. 65, no. 10, pp. 7888–7899, Oct. 2018.
[31] M. A. Azzouz and E. F. El-Saadany, "Multivariable grid admittance identification for impedance stabilization of active distribution networks," *IEEE Trans. Smart Grid*, vol. 8, no. 3, pp. 1116–1128, May 2017.
[32] R. Teodorescu, M. Liserre, and P. Rodriguez, *Grid Converters for Photovoltaic and Wind Power Systems*, vol. 29. New York, NY, USA: Wiley, 2011.
[33] N. Mohammed, M. Ciobotaru, and G. Town, "Online parametric estimation of grid impedance under unbalanced grid conditions," *Energies*, vol. 12, no. 24, 2019, Art. no. 4752.
[34] R. Rosso, J. Cassoli, G. Buticchi, S. Engelken, and M. Liserre, "Robust stability analysis of LCL filter based synchronverter under different grid conditions," in *IEEE Trans. Power Electron.*, vol. 34, no. 6, pp. 5842–5853, Jun. 2019.
[35] European Low Voltage Test Feeder. [Online] Available: http://sites.ieee.org/pes-testfeeders/
[36] Y. Han, H. Li, P. Shen, E. A. A. Coelho, and J. M. Guerrero, "Review of active and reactive power sharing strategies in hierarchical controlled microgrids," *IEEE Trans. Power Electron.*, vol. 32, no. 3, pp. 2427–2451, Mar. 2017.
[37] T. Suntio, T. Messo, and J. Puukko, *Power Electronic Converters: Dynamics and Control in Conventional and Renewable Energy Applications*. Weinheim, Germany: Wiley-VCH, 2017.

**Nabil Mohammed** (Student Member, IEEE) received the bachelor's degree in electrical power engineering from Tishreen University, Lattakia, Syria, and M.Eng. degree in electrical-mechatronics and automatic control from Universiti Teknologi Malaysia (UTM), Johor Bahru, Malaysia, in 2013 and 2017, respectively. He is currently working toward the Ph.D. degree in power electronics and photovoltaic power systems with Macquarie University, Macquarie Park, NSW, Australia.

In Summer 2019, he was a Visiting Researcher with the Department of Energy Technology, Aalborg University, Denmark. His research interests include power electronics converters, microgrids, smart grids, energy storage systems, adaptive control of power electronics inverters, system identification of grid impedance, and the PLC and SCADA applications to renewable energy systems.

**Tamas Kerekes** (Senior Member, IEEE) received the Diploma in electrical engineering, specializing in electric drives and robots, from the Technical University of Cluj, Romania, in 2002, and the M.Sc. degree in power electronics and drives and the Ph.D. degree from the Department of Energy Technology, Aalborg University, Aalborg, Denmark, in 2005 and 2009, respectively.

He is currently working with the Aalborg University, as an Associate Professor. His research focused on analysis and modeling of transformerless PV inverter systems. His research interests include grid connected renewable energy systems focusing on different grid forming and grid following control algorithms for power electronic converters for renewable energy systems with storage solutions.

**Mihai Ciobotaru** (Senior Member, IEEE) received the Diploma and the M.Eng. degree from the University of Galati, Galati, Romania, in 2002 and 2003, respectively, and the Ph.D. degree from Aalborg University, Aalborg, Denmark, in 2009, all in electrical engineering.

He was with the University of Galati, as an Associate Lecturer, until 2004, and with Aalborg University as an Associate Research Fellow, until 2010. He joined as a Research Fellow with the University of New South Wales, Sydney, NSW, Australia, where he worked as a Senior Research Fellow, until 2018. Thereafter, he joined Macquarie University, Sydney, NSW, Australia, where he currently works as a Senior Lecturer with the School of Engineering. His main research interests include power electronic inverters, power management of hybrid energy storage systems, module-level power electronics for photovoltaic systems, and dc distribution networks for more electric aircrafts.